Size Controllable and Surface Tunable Zeolitic Imidazolate Framework-8−Poly(acrylic acid sodium salt) Nanocomposites for pH Responsive Drug Release and Enhanced *in Vivo* Cancer Treatment

Li Yan,[†,§] Xianfeng Chen,*,[‡] Zhigang Wang,[#] Xiujuan Zhang,[⊥] Xiaoyue Zhu,[§] Mengjiao Zhou,[⊥] Wei Chen,[§] Longbiao Huang,[§] Vellaisamy A. L. Roy,[§] Peter K. N. Yu,[∥] Guangyu Zhu,[#] and Wenjun Zhang*,[§]

[†]Antibiotics Research and Re-evaluation Key Laboratory of Sichuan Province, Sichuan Industrial Institute of Antibiotics (SIIA), Chengdu University, Chengdu, Sichuan 610052, People's Republic of China

[‡]School of Engineering, Institute for Bioengineering, The University of Edinburgh, Mayfield Road, Edinburgh EH9 3JL, United Kingdom

[§]Center of Super-Diamond and Advanced Films (COSDAF) and Department of Materials Science and Engineering, City University of Hong Kong, Hong Kong SAR

[∥]Department of Physics, City University of Hong Kong, Hong Kong SAR

[⊥]Institute of Functional Nano & Soft Materials (FUNSOM) and Collaborative Innovation Center of Suzhou Nano Science and Technology, Jiangsu Key Laboratory for Carbon-Based Functional Materials & Devices, Soochow University, Suzhou, Jiangsu 215123, People's Republic of China

[#]Department of Chemistry, City University of Hong Kong, Hong Kong SAR

S *Supporting Information*
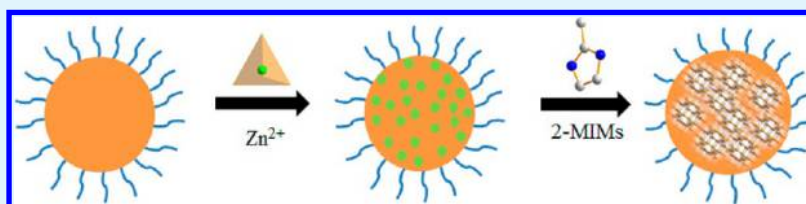
ABSTRACT: Nanoscale size controllable and surface modifiable zeolitic imidazolate framework-8−poly(acrylic acid sodium salt) (ZIF-8−PAAS) nanocomposites are fabricated by employing PAAS nanospheres as a soft template. These ZIF-8−PAAS nanocomposites have different sizes ranging from 30 to 200 nm and exhibit different crystallinity, and pH sensitivity. These nanocomposites can be employed as vectors to deliver doxorubicin for anticancer therapy, leading to greatly enhanced drug therapeutic efficacy when tested in cell lines and mice model. Systematic toxicity investigation including hematoxylin and eosin staining analysis of tumor and major organs, hematology analysis, and blood chemistry analysis indicates that the nanocomposites possess high biocompatibility. This work provides a strategy to make metal−organic frameworks (MOFs) nanocomposites with size tunability in nanoscale and flexible surface modification for various applications.

KEYWORDS: *metal−organic frameworks, nanomaterials, ZIF-8, nanocomposites, drug delivery*

1. INTRODUCTION

Crystalline metal−organic frameworks (MOFs) are fabricated by reticular synthesis, in which strong bonds are formed between metal ions (inorganic) and organic linker molecules.[1,2] As an emerging crystalline material, MOFs exhibit up to 90% free volume porosity and possess a surface area of over 6000 m^2/g.[3] With extraordinary flexibility of selection of organic and inorganic components (more than 20,000 kinds), MOFs can be rationally tuned with versatile structure, surface area, pore size, and property.[4−7] Because of these superior characteristics, MOFs have been widely used for air purification,[8−10] gas separations/storage,[11−14] chemical sensors,[15,16] heterogeneous catalysis,[17−20] and biomedical engineering.[21−28]

For many applications, it is of great importance to rationally design MOFs with optimal surface chemistry and size tunability. Taking drug delivery as an example, MOFs were first used as a drug carrier in 2006.[29,30] Since then, MOFs have been developed to a nanoregime of below 200 nm for improved drug delivery and bioimaging because materials within this size range can have high cellular uptake and long blood-circulation time[31,32] and these make them good candidates as drug carriers.[33−38] Despite the progress in recent years of using

nanoscale MOFs (NMOFs) for drug delivery, negligible work has been reported to produce size controllable NMOFs. Very recently, Park et al. reported production of size controllable (30−190 nm) Zr(IV)-based porphyrinic MOFs by adjusting the concentration of reactant benzoic acid. The results demonstrated that the MOFs with a size of 90 nm have significantly higher cellular uptake and *in vivo* photodynamic therapy efficacy when used to deliver a photosensitizer than those of other sizes.[39] However, the specific parameters controlling the size of MOFs need to be tuned for each type of material. Beyond size controllability, the surfaces of nanomaterials play an important role in biological and medical applications. Currently, stabilization of MOFs in aqueous solution is predominantly reliant on surface coating, but the conventional polymer or silica coating may block the pores on the surface of MOFs, leading to a decrease of porosity and correspondingly drug loading capacity.[40]

To address these bottlenecks of making size controllable and surface tunable NMOFs for efficient drug delivery, herein, we propose a method of employing poly(acrylic acid sodium salt) (PAAS) nanospheres as a soft template to produce size controllable and surface modifiable zeolitic imidazolate framework-8−poly(acrylic acid sodium salt) (ZIF-8−PAAS) nanocomposites. In this unique approach, we hypothesize that the particle size can be precisely controlled by the molecular weight of the PAAS soft template; and instead of directly modifying MOFs for stabilization, the surface modification may be constructed on the PAAS template. To confirm our hypothesis, we systematically studied the approach of using PAAS as templates for synthesizing NMOFs with controllable sizes of below 200 nm and establishing desirable surface modification on PAAS. Through extensive studies, we found that surface modification molecules should be conjugated to PAAS first and then the conjugated polymer be used as a template for MOFs growth. In this way, NMOFs with high stability and cancer cell targeting ability can be conveniently synthesized. Because surface modification was performed to the PAAS template, it is expected that the high porosity of NMOFs and corresponding drug loading capacity can be retained without being negatively affected by surface modification. To the best of our knowledge, such an approach of using PAAS of different molecular weights to produce NMOFs with size controllability and desirable surface modification has not been reported. After successful preparation of NMOFs, the size, morphology, structure, drug loading, and release under different conditions, *in vitro* cancer cell killing efficiency, and *in vivo* tumor inhibition rate and biosafety profiles were investigated in detail. The experimental results demonstrate that these NMOFs possess superior characteristics of high drug loading capacity, pH responsive drug release, excellent tumor inhibition efficacy, and great biocompatibility. Overall, this soft-template method provides a powerful approach to fabricate size and surface controllable NMOFs for high-performance applications.

2. EXPERIMENTAL SECTION

2.1. Materials and Characterization. PAAS (M_w = 20K), isopropyl alcohol, and methanol were purchased from International Laboratory (USA). Zn(NO$_3$)$_2$ and 2-methylimidazole were ordered from Acros (USA). PAAS (M_w = 8K), PAAS (M_w = 1.2K), and poly(ethylene glycol) (PEG)−amine (M_w = 5000) were bought from Sigma-Aldrich (USA). Doxorubicin (DOX) was from Beijing Zhongshuo Pharmaceutical Technology Development Co., Ltd. (China). Dulbecco's modified Eagle medium (DMEM), fetal bovine serum (FBS), phosphate-buffered saline (PBS), MTT (3-(4,5-dimethylthiazol-2-yl)-2,5-diphenyltetrazolium bromide), penicillin/streptomycin, and Hoechst 33342 were obtained from Life Technologies (USA). Cell culture 96-well plates and dishes were obtained from Corning (USA). ζ potential and size distribution were measured by Zetasizer (Malvern). Transmission electron microscopy (TEM) and high-resolution transmission electron microscopy (HRTEM) images were taken on Technai 12 (Philips) and JEOL JEM 2100F, respectively. Scanning electron microscopy (SEM) images were taken on an FEG SEM-XL30. Powder X-ray diffraction (XRD) patterns were collected with D2 Phaser X-ray diffraction using Cu Kα radiation.

2.2. PAAS Nanosphere Fabrication. PAAS (M_w = 1.2K, 8K, and 20K) solutions were first diluted to 0.2 g/mL, and then 200 μL of the diluted PAAS solutions (M_w 1.2K, 8K, and 20K) were added separately into 4 mL of Milli-Q water (18.2 mΩ) with 5 min stirring. Subsequently, 20, 40, and 80 mL aliquots of isopropyl alcohol were added into PAAS solutions with molecular weights of 1.2K, 8K, and 20K, respectively, with magnetic stirring for making different sizes of PAAS templates.

2.3. ZIF-8-PAAS Nanocomposites Fabrication. The as-prepared PAAS nanospheres were mixed with 6.7 mL of 0.1 M Zn(NO$_3$)$_2$ in methanol solution under stirring for 5 min. Then, the mixture was centrifuged at 2000, 4000, and 6000 rpm for PAAS with M_w = 1.2K, 8K, and 20K, respectively. Next, the precipitated PAA-Zn nanospheres were re-dispersed in 20 mL of methanol, followed by addition of 20 mL of 20 mg/mL 2-methylimidazole in methanol under stirring. Finally, the solution was subjected to reaction at 70 °C for 12 h.

2.4. PEG Modified ZIF-8 NMOFs Nanocomposites Fabrication. First, 300 μL of 0.2 g/mL PAAS (M_w = 8K) solution and 1.5 mL of 2 mg/mL PEG−amine were sequentially added into 1.5 mL of Milli-Q water (18.2 mΩ), followed by overnight stirring in the presence of EDC as a catalyst. Second, 3 mL of Milli-Q water and 24 mL of isopropyl alcohol were added into the solution with magnetic stirring. Third, 8 mL of 0.1 M Zn(NO$_3$)$_2$ in methanol solution was added and stirred for 5 min. Fourth, the mixture was centrifuged at 10000 rpm for 30 min. Fifth, the precipitation was re-dispersed in 4 mL of methanol, followed by addition of 16 mL of 20 mg/mL 2-methylimidazole in methanol under active stirring. Finally, the solution was subjected to reaction at 70 °C for 12 h.

2.5. Drug Loading Capacity and Loading Efficiency. Solutions of 400, 200, 100, 50, and 25 μL of 2 mg/mL ZIF-8 NMOFs nanocomposites were added into 200 μL of 2 mg/mL DOX solution, and the mixtures were under stirring for 24 h. The amount of drug loading was determined from the absorbance differences (at 480 nm) of DOX in the solution before and after mixing with ZIF-8 NMOFs nanocomposites. Loading capacity and loading efficiency were calculated by the following equations: (1) loading capacity = $[(W_t − W_f)/W_n] × 100\%$ and (2) loading efficiency = $[(W_t − W_f)/W_t] × 100\%$, where W_t is the total DOX in solution, W_f the free DOX after loading, and W_n the weight of ZIF-8 NMOFs nanocomposites.

2.6. *In Vitro* DOX Release Profile. DOX loaded ZIF-8 NMOFs nanocomposites were added into 2 mL of buffer solution (pH = 7.4 and pH = 5) placed on a shaking water bath at 37 °C. After different time intervals, 120 μL of the buffer solution was collected and the amount of DOX release was measured by absorbance at 480 nm.

2.7. Fluorescence Microscopy. HeLa cell suspension was seeded onto a sterile glass coverslip in a 35 mm tissue culture dish for 24 h. Then the cell culture medium was replaced with a fresh medium containing DOX loaded ZIF-8 NMOFs nanocomposites (10 wt % DOX) at DOX concentration of 4 μg/mL. At 4 h after incubation, the nuclei were stained by Hoechst 33342 and the coverslip was mounted onto a glass slide for fluorescence microscopy.

2.8. Cell Viability Measurement. HeLa cells were washed twice with PBS. HeLa cells suspended in DMEM (with 10% FBS and 1% penicillin/streptomycin) were plated into 96-well plates (100 μL of DMEM and 1,500−3,000 cells per well). The cells were incubated at 37 °C for 24 h before further treatment. Then, another 100 μL of DMEM containing various concentrations of DOX, ZIF-8 NMOFs nanocomposites, and DOX loaded ZIF-8 NMOFs nanocomposites

Scheme 1. Schematic Illustration of the Approach of Synthesizing ZIF-8 NMOFs Nanocomposites Using PAAS as a Soft Template
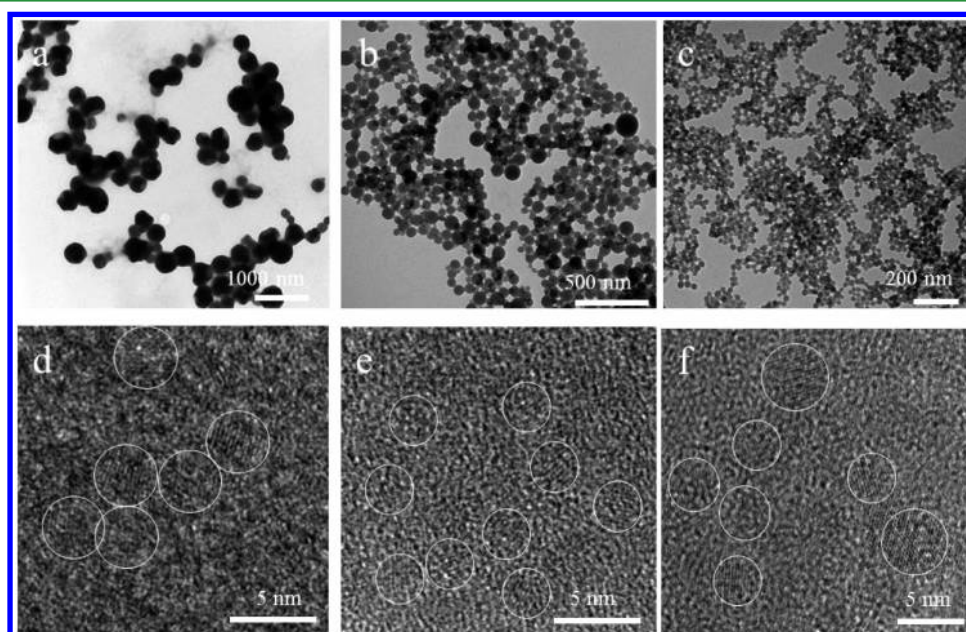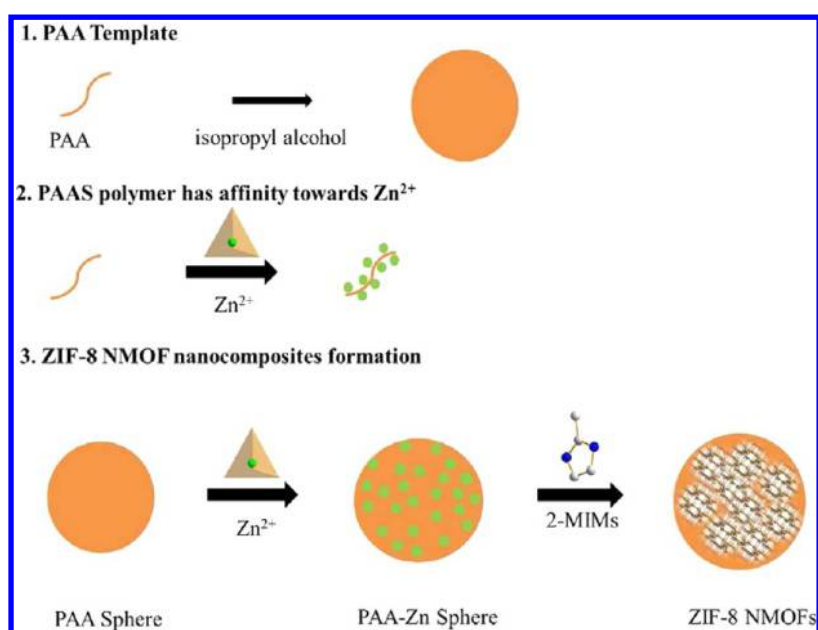

Figure 1. (a−c) TEM and (d−f) HRTEM images of (a, d) ZIF-8 (1.2K), (b, e) ZIF-8 (8K), and (c, f) ZIF-8 (20K) NMOFs nanocomposites.

were added into 96-well plates for additional 48 and 72 h incubation. After incubation, the original medium in each well was removed. Subsequently, 180 μL of DMEM (without FBS) and 20 μL of MTT stock solution (5 mg/mL in PBS) were added and incubated for 4 h. Then the medium containing MTT was completely removed, followed by adding 200 μL of dimethyl sulfoxide (DMSO) to each well. Cell viabilities were determined by reading the absorbance of the plates at 540 nm using a BioTek Powerwave XS microplate reader.

2.9. *In Vivo* Cancer Therapy. The tumor model was developed by injection of 4T1 cells to Balb/C mice (2.5 × 10^6 4T1 cells in 100 μL of PBS). At 7 days after inoculation of the cancer cells, the mice were randomly divided into four groups (n = 4; defined as treatment day 1). Then 200 μL of different drug formulations at a dose of 2.5 mg/mL DOX (referred to as MOF-DOX PEG, MOF-DOX, and DOX) and PBS solution were injected into the different groups of mice *via* the tail vein on treatment days 1, 7, 13, and 19. The tumor size and body

weight were monitored at 3 day intervals until day 22. The tumor size was calculated according to the following equation: volume = (tumor length) × (tumor width)^2/2. For biosafety evaluation, 200 μL of different drug formulations were injected to healthy mice via the tail vein at day 1, and then major organs including heart, liver, spleen, lung, and kidney as well as tumor were harvested. All tissues were fixed in a 10% formalin solution, embedded in paraffin, sectioned, and stained with hematoxylin and eosin (H&E) for analysis. All experiments were performed in compliance with the National Act on the Use of Experimental Animals (China) and the guidelines issued by Sichuan Province and Chengdu University. All experiments were approved by the Animal Ethics Committee of Chengdu University.
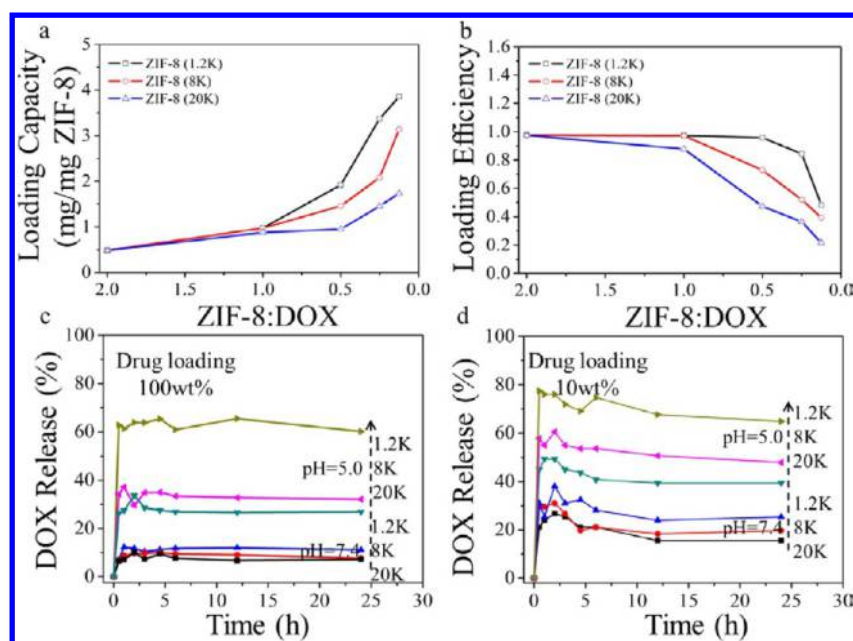
Figure 2. (a) Loading capacities and (b) loading efficiencies of DOX to ZIF-8 NMOFs nanocomposites at different mixing ratios (five groups of ZIF-8 NMOFs nanocomposites to DOX ratios: 2:1, 1:1, 1:2, 1:4, and 1:8); (c, d) DOX release curves at pH 7.4 (physiological pH value) and pH 5 from ZIF NMOFs nanocomposites with drug loading capacity of (c) 100 and (d) 10 wt %.

3. RESULTS AND DISCUSSION

3.1. ZIF-8 NMOFs Nanocomposites Preparation and Characterization. In our study, PAAS nanospheres were synthesized by a deionized water−isopropyl alcohol approach.[41] PAAS with three different molecular weights (M_w) of 1.2K, 8K, and 20K were chosen in the preparation. We found that PAAS nanospheres of different sizes of 105, 79, and 33 nm were formed by self-assembly from PAAS with M_w = 1.2K, 8K, and 20K, respectively. The sizes of the nanospheres were measured by dynamic light scattering (DLS; Supporting Information Figure S1). SEM also confirms that PAAS nanospheres sizes are around 80 and 35 nm for PAAS with M_w of 8K and 20K, respectively (Supporting Information Figure S2 and Figure S3). Because Zn^{2+} has higher affinity toward -COO$^-$ groups in PAAS polymer chains than Na$^+$, PAAS nanospheres were mixed with $Zn(NO_3)_2$ at room temperature for 5 min so that Zn^{2+} could replace Na$^+$ (Scheme 1). The as-prepared PAA−Zn nanospheres were then reacted with 2-methylimidazole (2-MIMs) to form ZIF-8−PAAS crystal using the Zn^{2+} adsorbed on PAA−Zn nanopheres as the Zn source. The size of ZIF-8−PAAS nanocomposites can be controlled from 200 and 90 to 30 nm by using PAAS nanosphere templates prepared from PAAS molecules with M_w = 1.2K, 8K, and 20K, respectively. Depending on the molecular weight of the used PAAS, the produced nanocomposites are denoted as ZIF-8 (1.2K), ZIF-8 (8K), and ZIF-8 (20K). The corresponding TEM images are presented in Figure 1a−c. The SEM images in Supporting Information Figure S4 show that ZIF-8 NMOFs nanocomposites fabricated from different PAAS nanospheres possess similar morphology. The sizes of these different ZIF-8 NMOFs nanocomposites were also confirmed by DLS analysis, which shows the diameters of ZIF-8 (1.2K), ZIF-8 (8K), and ZIF-8 (20K) particles are approximately 190, 98, and 46 nm, respectively. (Supporting Information Figure S5) The obtained ZIF-8 (1.2K), ZIF-8 (8K), and ZIF-8 (20K) NMOFs nanocomposites exhibit negative charge because of -COO$^-$ groups in the PAAS, which were measured by DLS

analysis (Supporting Information Figure S6). Fourier transform infrared spectroscopy (FTIR) results show the carbonyl stretching vibration of -COO$^-$ at 1580 cm^{-1} and the stretching vibration of -COOH at 1717 cm^{-1}, which confirms the existence of -COO$^-$ groups in the nanocomposites (Supporting Information Figure S7).

To determine the crystal structure of ZIF-8 NMOFs nanocomposites, XRD was performed (Supporting Information Figure S8). From the XRD pattern, one can observe that the diffraction patterns of ZIF-8 (1.2K), ZIF-8 (8K), and ZIF-8 (20K) nanocomposites have matched characteristic peaks, suggesting the formation of ZIF-8 crystals. The peaks of the XRD pattern of ZIF-8 (20K) are much sharper and stronger in intensity than those of ZIF-8 (1.2K) and ZIF-8 (8K). This indicates that ZIF-8 (20K) NMOFs nanocomposites possess higher crystallinity than ZIF-8 (8K) and ZIF-8 (1.2K) ones. To further investigate the difference in crystallinity, HRTEM was carried out (Figure 1d−f and Supporting Information Figure S9). From the results, we can find that ZIF-8 (1.2K), ZIF-8 (8K), and ZIF-8 (20K) nanocomposites contain a crystalline region and an amorphous area. Instead, ZIF-8 nanocrystals of a few nanometers are well-dispersed within the PAAS matrix. It is worth noting that, from the HRTEM images, ZIF-8 (20K) NMOFs nanocomposites possess a more well-aligned and larger crystalline region than the ZIF-8 (8K) and ZIF-8 (1.2K) ones, which is in correspondence with the XRD results. Therefore, we can conclude that our method is able to control the crystallinity of fabricated ZIF-8 NMOFs nanocomposites. The energy-dispersive X-ray spectroscopy (EDX) mapping images of ZIF-8 (1.2K) and ZIF-8 (8K) NMOFs nanocomposites demonstrate the Zn element is well-distributed across the nanoparticles, confirming the relatively homogeneous composition (Supporting Information Figure S10 and Figure S11).

3.2. *In Vitro* Study of ZIF-8 NMOFs Nanocomposites. After successful preparation of ZIF-8 NMOFs nanocomposites with different sizes, their drug loading and release capabilities

were evaluated. DOX, a well-known anticancer drug, was used as a test case. DOX loading was achieved by simply mixing ZIF-8 NMOFs nanocomposites with DOX in an aqueous solution. Because the pore size of ZIF-8 is very small, DOX is physically adsorbed on the surface of the ZIF-8 nanocomposites. We found that the drug loading capability of the three prepared ZIF-8 NMOFs nanocomposites was different. ZIF-8 (1.2K) NMOFs nanocomposites show much better DOX loading capacity than ZIF-8 (8K) and ZIF-8 (20K) ones (Figure 2a,b). When the mixing ratio of ZIF-8 NMOFs nanocomposites to DOX is 1:1, the loading efficiencies (weight of loaded DOX/ weight of total DOX) are >97% for ZIF-8 (1.2K) and ZIF-8 (8K) and >87% for ZIF-8 (20K). When the amount of DOX continually increases in the mixture (ZIF-8 to DOX ratios drop to 1:2, 1:4, and 1:8), the loading efficiency drops as the percentage of ZIF-8 NMOFs nanocomposites in the mixture becomes smaller. However, the loading capacity (weight of loaded DOX/weight of ZIF-8) keeps increasing. For example, when the ratio of ZIF-8 NMOFs nanocomposites to DOX is 1:8, every milligram of ZIF-8 (1.2K), ZIF-8 (8K), and ZIF-8 (20K) can load 3.85 (385%), 3.14 (314%), and 1.73 (173%) mg of DOX, with loading efficiencies of 48%, 39%, and 22%, respectively. These values indicate that our fabricated ZIF-8 NMOFs nanocomposites show very high drug loading capacity. The differences of drug loading capacity may be caused by the different crystallinities of the different ZIF-8 NMOFs nanocomposites.

Once confirming that our fabricated ZIF-8 NMOFs nanocomposites display excellent drug loading capacity, we next investigated their release kinetics. ZIF-8 (1.2K), ZIF-8 (8K), and ZIF-8 (20K) NMOFs nanocomposites with drug loading capacity of 100 wt % (the weight of drug and ZIF-8 is equivalent) and 10 wt % (weight of drug/weight of ZIF-8 = 1:10) were selected for *in vitro* release study (Figure 2c,d). Under pH 7.4, all ZIF NMOFs nanocomposites can hold DOX molecule relatively firmly for at least 24 h, with only <15% (drug loading, 100 wt %) and <30% (drug loading, 10 wt %) of the loaded drugs released to the buffer solutions. However, when pH drops to 5 (the pH value of tumor tissue or lysosome), drug release becomes faster. Interestingly, these as-fabricated ZIF-8 NMOFs nanocomposites display different pH sensitivities. ZIF-8 (1.2K) is found to be more pH sensitive than ZIF-8 (8K) and ZIF-8 (20K). For example, ZIF-8 (1.2K) NMOFs nanocomposites with drug loading capacity of 100 wt % releases greater than 60% of DOX at pH 5, which is much higher than the other two nanocomposites. The possible explanation of the different pH sensitivity is due to the different crystallinity: ZIF (1.2K) NMOFs nanocomposites have less crystallinity than ZIF-8 (8K) and ZIF-8 (20K), resulting in lower stability in acid environments, and thus release of more DOX drug. This explanation was supported by TEM images of ZIF-8 NMOFs nanocomposites after treatment in pH 7.4 and pH 5 buffer solutions. The structures of the vast majority of ZIF-8 (1.2K), ZIF-8 (8K), and ZIF-8 (20K) NMOFs nanocomposites collapse at pH 5, while their structures are relatively stable at pH 7.4, particularly for ZIF-8 (8K) and ZIF-8 (20K); at pH 5, some ZIF-8 (20K) NMOFs nanocomposites can still maintain the structure (Supporting Information Figure S12). Consistent with these findings observed from TEM, DLS shows the mean count rates of ZIF-8 (1.2K), ZIF-8 (8K), and ZIF-8 (20K) NMOFs nanocomposites significantly drop to less than 20 kcps (almost background level) after pH 5 buffer treatment for 2 min. This means that the release of the drug

from the MOFs is more efficient at a lower pH value. Overall, ZIF-8 (1.2K), ZIF-8 (8K), and ZIF-8 (20K) NMOFs nanocomposites display different sizes, crystallinities, drug loading capacities, and pH sensitivities (Table 1).

Table 1. Summary of Sizes and Loading Capacities of PAAS and ZIF-8 NMOFs Nanocomposites

	PAAS (1.2K)	PAAS (8K)	PAAS (20K)
PAAS size (nm; DLS)	105	79	33
ZIF-8 size (nm; DLS)	190	98	46
ZIF-8 size (nm; TEM)	200	90	30
drug loading capacity (wt %)	385	314	173

Following the study of the release kinetics, the intracellular delivery of different sizes of ZIF-8 NMOFs nanocomposites loaded with DOX was studied, because the size of nanomaterials can dramatically affect their intracellular delivery efficiency. In this study, we selected ZIF-8 NMOFs nanocomposites with DOX loading of 10 wt % to investigate the intracellular delivery efficiencies of the three different ZIF-8 NMOFs nanocomposites. The results are shown in Figure 3. It is apparent that the intracellular delivery efficiency is size dependent: ZIF-8 (1.2K) < ZIF-8 (8K) < ZIF-8 (20K). After 4 h incubation, the HeLa cells treated with ZIF-8 (20K) (46 nm) NMOFs nanocomposites show a much stronger fluorescence signal from DOX than those treated with ZIF-8 (1.2K) (190 nm) and ZIF-8 (8K) (98 nm) NMOFs nanocomposites.

Subsequently, we characterized the HeLa cell viability after incubation with ZIF-8 (1.2K), ZIF-8 (8K), and ZIF-8 (20K) NMOFs nanocomposites for 48 and 72 h (Figure 4). Again, we chose ZIF-8 NMOFs nanocomposites with 10 wt % DOX loading for testing. The results show that significantly improved delivery efficiency can be achieved with the aid of ZIF-8 NMOFs nanocomposites, particularly with the nanocomposites made from PAAS of molecular weight of 20K Da (Figure 4). This is well-matched with our data showing that ZIF-8 (20K) enter cells more efficiently than ZIF-8 (1.2K) and ZIF-8 (8K) NMOFs nanocomposites. For ZIF-8 (1.2K) and ZIF-8 (8K) NMOFs nanocomposites, the drug efficacy is overall comparable to free DOX in cell lines, depending on the concentrations of the drug. However, we expect that the ZIF-8−DOX can realize much better efficacy and smaller side effect in *in vivo* applications due to the enhanced permeability and retention (EPR) effect and the preferable release kinetics of nanomedicine.

3.3. *In Vivo* Study of ZIF-8 NMOFs Nanocomposites. Once we knew that ZIF-8 NMOFs nanocomposites have excellent properties and high cell killing efficiency, their application in *in vivo* anticancer therapy was next evaluated. In this study, ZIF-8 (8K) NMOFs nanocomposites were chosen as a drug delivery vector, because of its well-balanced drug loading capacity, pH sensitivity, and stability. In order to prolong the material's blood-circulation time, PEG (M_w = 5000) was conjugated to PAAS (8K) molecule before nanocomposites fabrication (Scheme 2 and Figure S13). Then for drug loading, 1 mL of 1 mg/mL DOX was mixed with 1 mL of 1 mg/mL MOF-PEG nanocomposites for 24 h. During this process, almost all DOX was able to be loaded to MOF-PEG nanocomposites. This is the advantage of our ZIF-8 nanocomposites. The reason is PEG is conjugated to a PAAS template instead of ZIF-8 nanocrystal, and therefore it does not interfere with subsequent drug loading.
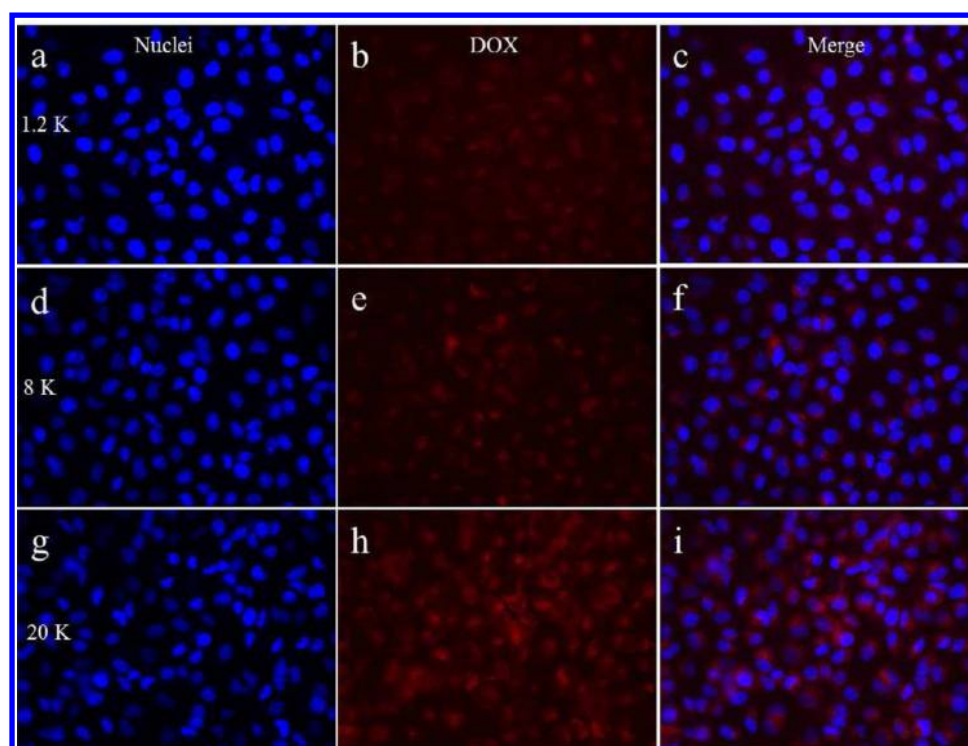
Figure 3. (a–i) Fluorescence microscopy images of HeLa cells after 4 h incubation with (a–c) ZIF-8 (1.2*K*), (d–f) ZIF-8 (8*K*), and (g–i) ZIF-8 (20*K*) NMOFs nanocomposites loaded with 10 wt % DOX.
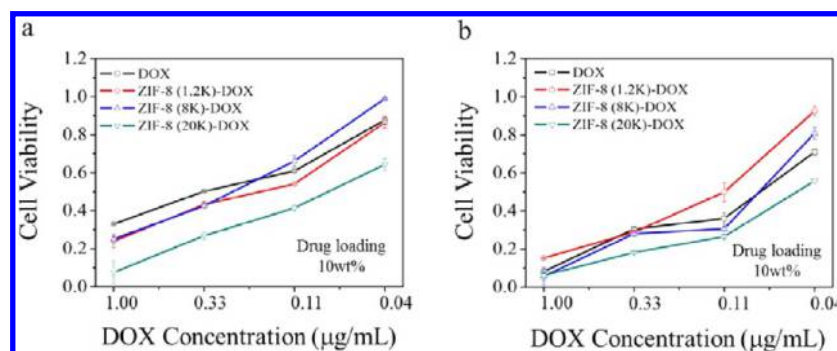

Figure 4. Viabilities of HeLa cells after 48 (a) and 72 h (b) of incubation with free DOX and ZIF-8 (1.2*K*), ZIF-8 (8*K*), and ZIF-8 (20*K*) NMOFs nanocomposites loaded with 10 wt % DOX.

After drug loading, the biodistribution of MOF-PEG DOX nanocomposites in mice was investigated by using a small animal *in vivo* fluorescence system to detect the fluorescence signal of DOX (Supporting Information Figure S15). It was found that DOX can be effectively delivered to the tumor site within 24 h, demonstrated by the very bright DOX fluorescence signal. At 48 h after injection, the fluorescence intensity in the tumor site further increased, while the fluorescence intensities in major organs including heart, liver, kidney, spleen, and lung starting to drop.

Since PEG modified MOF nanocomposites can effectively deliver DOX to tumor sites, it is expected that it can efficiently inhibit tumor growth. To verify this, a group of five mice was intravenously injected with MOF-PEG DOX (DOX dose at 2.5 mg/kg) and then the tumor volumes of the mice were monitored for 22 days. In addition, for comparison purposes, three other groups of mice were injected with PBS, free DOX (DOX), and MOF loaded with DOX but without PEG modification (MOF DOX). The results are shown in Figure 5a.

It is clear that the therapeutic efficacy of free DOX molecules and the DOX delivered by MOF nanocomposites without PEG surface modification is very low, indicated by the rapidly growing tumor during the observation period. In great comparison, MOF-PEG DOX constantly exhibits significantly improved therapeutic efficiency: more than 50% tumor reduction compared with the other three groups. There is a statistical difference between MOF-PEG DOX and other the three groups ($p < 0.05$). Moreover, there is minimal weight loss in the group treated with MOF-PEG DOX (Figure 5b), indicating that the PEG modified MOF with MTX has great therapeutic efficacy with good biocompatibility. In addition, H&E staining of tumor slices was also evaluated. From the H&E staining, higher tumor cell damage is shown in the MOF-PEG DOX treated tumor, compared with MOF DOX, DOX, and PBS treated groups, which confirms that MOF-PEG DOX has better anticancer efficiency (Figure 5c).

To investigate the mechanism of MOF-PEG DOX inhibition of tumor growth, immuno-histochemistry analysis of Caspase-3,

Scheme 2. Schematic Illustration of PEG Modified ZIF-8 NMOFs Nanocomposites Formation Using PAAS as a Soft Template
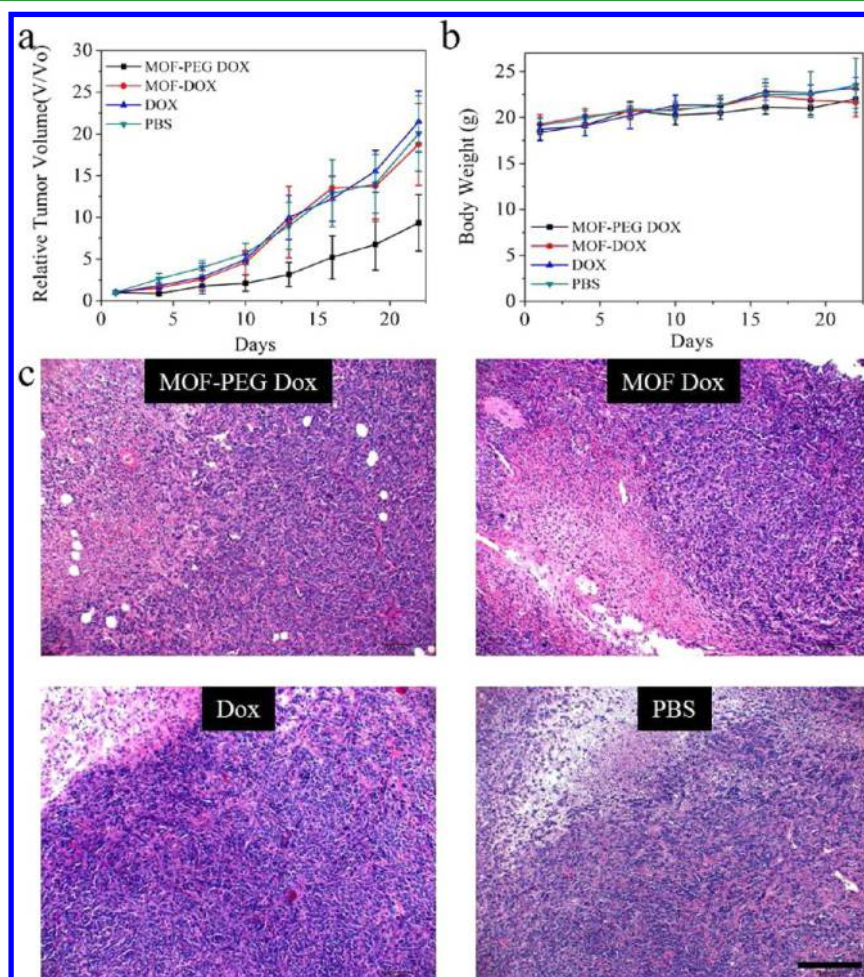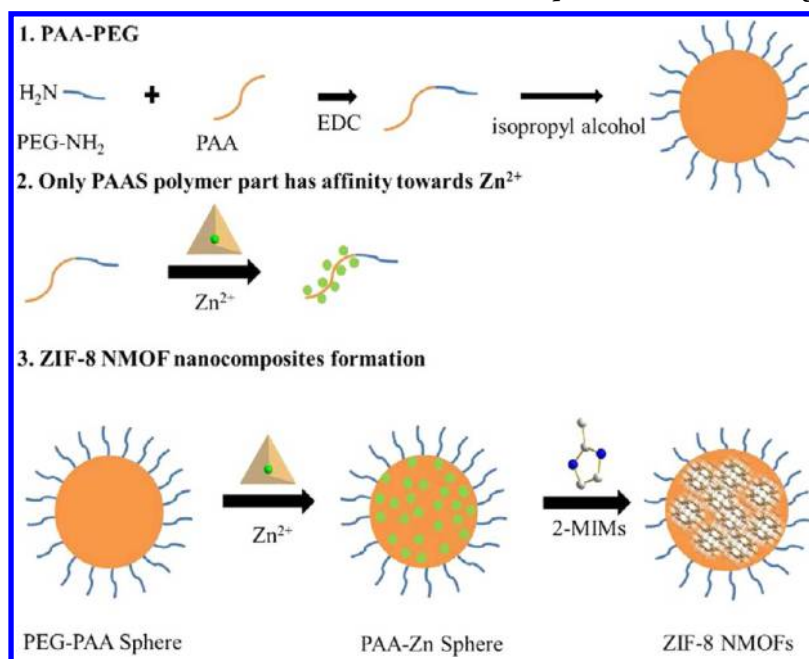

Figure 5. *In vivo* anticancer activities: (a) tumor growth curves of 4T1-tumor-bearing BALB/C mice after intravenous injection with (1) PBS, (2) DOX loaded by PEG modified ZIF-8 NMOFs nanocomposites (MOF-PEG DOX), (3) DOX loaded by ZIF-8 NMOFs nanocomposites (MOF DOX), and (4) free DOX; (b) body weight evolution of 4T1-tumor-bearing mice at different times after intravenous injection of different materials; (c) H&E staining images of tumors slices. Scale bar: 100 μm.
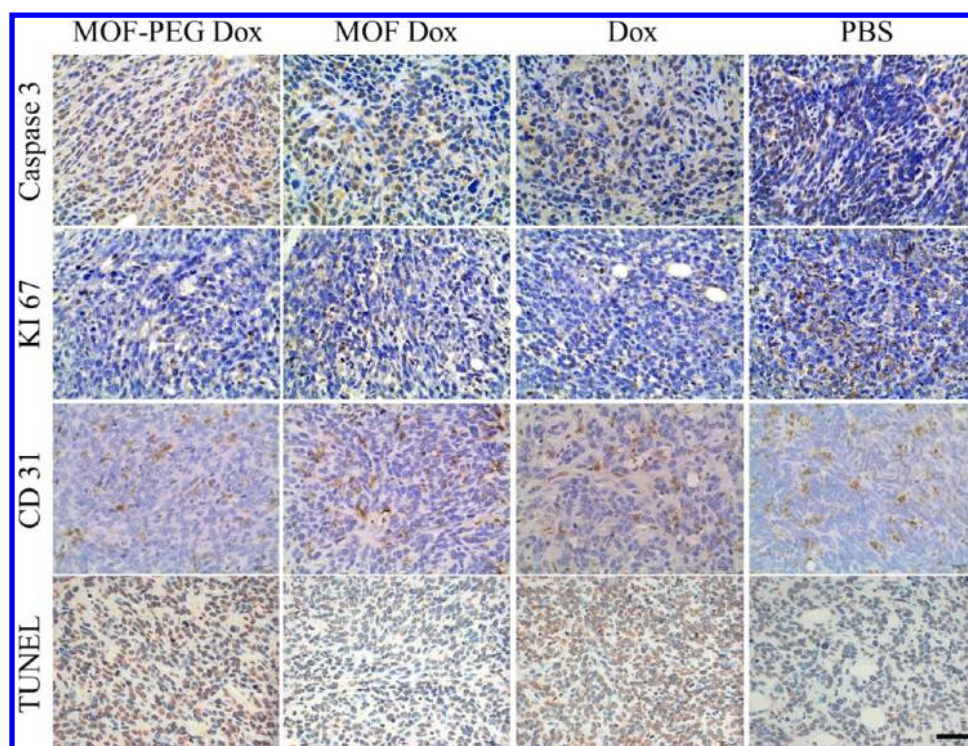
Figure 6. Immuno-histochemistry (Caspase 3, KI67, and CD31 antibody) and TUNEL images of tumor slices. 4T1-tumor-bearing BALB/C mice after intravenous injection with (1) DOX loaded by PEG modified ZIF-8 NMOFs nanocomposites (MOF-PEG DOX), (2) DOX loaded by ZIF-8 NMOFs nanocomposites (MOF DOX), (3) free DOX, and (4) PBS. Yellow brown indicates positive; blue indicates negative. Scale bar: 40 μm.

KI-67, and CD31 as well as terminal deoxynucleotidyl transferased dUTP nick end labeling (TUNEL) was conducted (Figure 6). Caspase-3, KI-67, and CD31 are the indicators for apoptosis, cell proliferation, and tumor angiogenesis, respectively. In Figure 6, the mean optical densities (MODs) for Caspase-3 expression are 0.313 ± 0.001, 0.300 ± 0.006, 0.288 ± 0.001, and 0.277 ± 0.004 for MOF-PEG DOX, MOF DOX, DOX, and PBS treated groups, respectively. The higher expression of Caspase-3 in the MOF-PEG DOX treated group indicates that MOF-PEG DOX induces higher cell apoptosis than MOF DOX and DOX, thereby causing the death of tumor cells. For quantity analysis, the cell apoptosis was also evaluated by TUNEL, which showed $73.3 \pm 4.04\%$, $34 \pm 7\%$, $69.0 \pm 2.6\%$, and $24.7 \pm 2.5\%$ apoptosis cells in MOF-PEG DOX, MOF DOX, DOX, and PBS treated groups, respectively. These confirm that MOF-PEG DOX can effectively kill tumor cells by inducing cell apoptosis.

In addition, we evaluated the level of KI-67, which is a key indicator for cell proliferation. Dramatically lowered expression of KI-67 was detected in MOF-PEG DOX treated tumor (MOD = 0.295 ± 0.013) compared with MOF DOX (MOD = 0.339 ± 0.013), DOX (MOD = 0.328 ± 0.016), and PBS (MOD = 0.345 ± 0.008) treated groups, indicating enhanced inhibition of the cancer cell proliferation. Finally, we analyzed CD31 protein, which is highly associated with tumor angiogenesis and tumor growth. In Figure 6, lower CD31 expression is presented in the MOF-PEG DOX treated group, revealing that tumor growth was effectively inhibited. Microvascular density (MVD) was also counted (most vascularized area; in every slice five hot spots were selected), which is highly associated with tumor metastasis and prognosis. The average MVD results are 6.6 ± 1.1, 12 ± 1.6, 10.4 ± 2.7, and 16.6 ± 2 in MOF-PEG DOX, MOF DOX, DOX, and PBS treated

groups, respectively. The MVD counting confirms the effectiveness of MOF-PEG DOX for tumor growth inhibition.

3.4. Biosafety Study of ZIF-8 NMOFs Nanocomposites. Biosafety is a major concern for clinical application of nanomedicine; therefore, we finally systematically investigated the toxicity of MOF-PEG DOX. First, histopathological examinations (H&E staining) were conducted to analyze major organs, including heart, liver, spleen, lung, and kidney (Figure 7). From these H&E staining images, no obvious organ damage is shown in DOX and MOF-PEG DOX treated groups. Apparently, histopathological examinations demonstrate MOF-PEG DOX nanocomposites cause minimal toxicity to major organs. Because liver and kidney damage is a very common side effect of therapeutic drugs, to investigate he biosafety of MOF-PEG DOX, the liver and kidney function (Figure 8) of the treated mice were evaluated by measuring the blood serum levels of alanine aminotransferase (ALT), aspartate aminotransferase (AST), alkaline phosphatase (ALP), blood urea nitrogen (BUN), creatinine (CRE), and uric acid (UA). From the results, no obvious abnormality is found, indicating that MOF-PEG DOX nanocomposites have low toxicity toward liver and kidney, which is in line with our histopathological results. Since ZIF-8 NMOFs were intravenously injected, these drugs directly interacted with blood. Therefore, blood chemistry analysis was performed. There is also no significant abnormality of the complete blood counts data, including red blood cells (RBC), white blood cells (WBC), hemoglobin (HGB), hematocrit (HCT), mean corpuscular volume (MCV), mean corpuscular hemoglobin (MCH), mean corpuscular hemoglobin concentration (MCHC), and platelet count (PLT) (Figure S16). Overall, all of these toxicity profiles suggest that MOF-PEG DOX has high biosafety for *in vivo* cancer therapy.
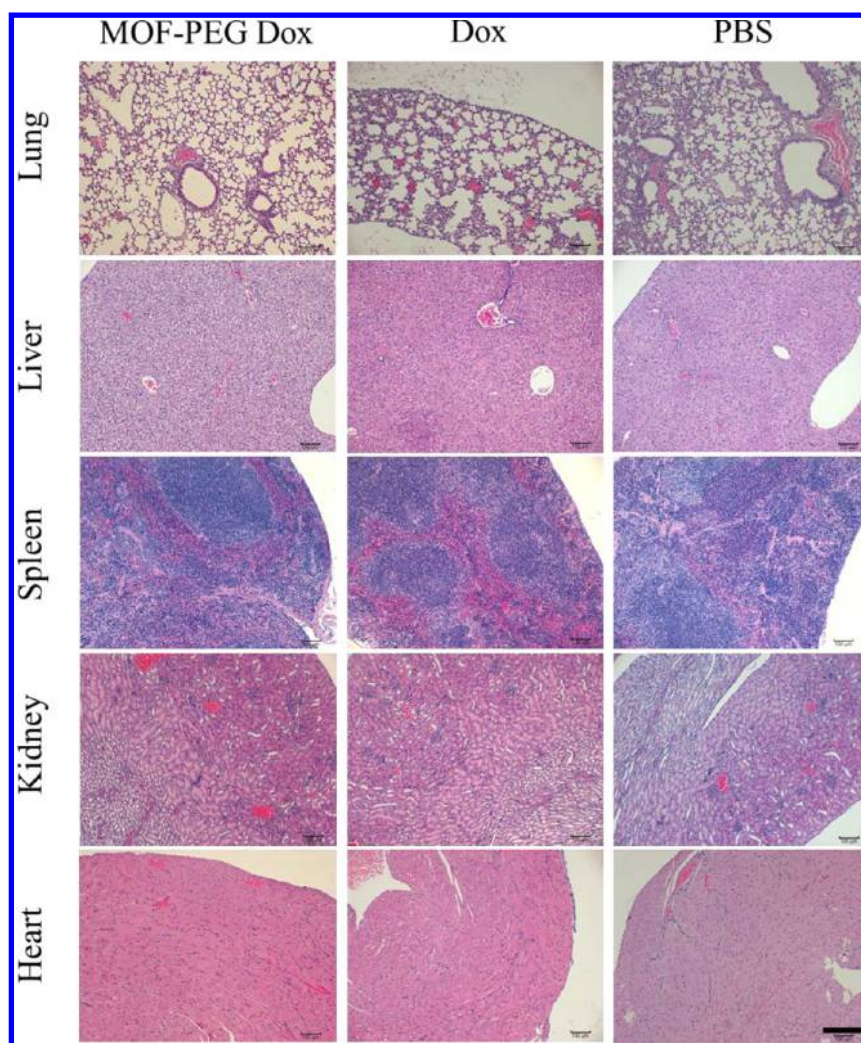
Figure 7. H&E staining images of major organs (heart, liver, spleen, lung, and kidney). The mice were treated with DOX loaded by PEG modified ZIF-8 NMOFs nanocomposites, free DOX, and PBS at day 1 and sacrificed at day 7. Scale bar: 200 μm.
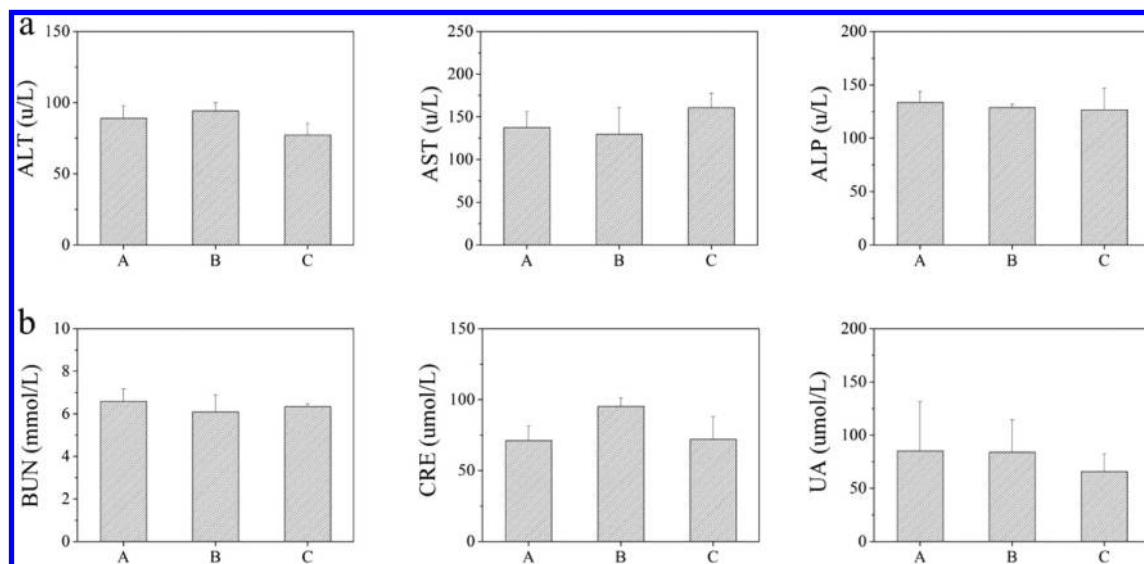

Figure 8. Liver function (ALT, AST, and ALP) and kidney function (BUN, CRE, and UA) of healthy mice. The mice were treated with (A) PBS, (B) free DOX, and (C) PEG modified ZIF-8 NMOFs nanocomposites at day 1 and sacrificed at day 7. The normal ranges of ALT, AST, ALP, BUN, CRE, and UA are 33.0−99.0, 69.5−210.0, 40.0−190.0, 2.00−7.70, 22.0−97.0, and 20−420, respectively.

4. CONCLUSION

In summary, we have developed a strategy of using PAAS as a soft template to prepare size controllable and surface modifiable ZIF-8-PAAS nanocomposites in the range of 30−200 nm which is suitable for drug delivery. The as-fabricated nanocomposites have ultrahigh drug loading capacity of up to 385 wt %. We also demonstrate that the nanocomposites fabricated from different PAAS nanospheres have different crystallinity, drug loading capacity, and release kinetics, and pH sensitivity. Also very importantly, these nanocomposites can be conveniently modified with functional molecules. As a test case, these nanocomposites were functionalized with PEG and employed as vectors to deliver DOX for cancer therapy with greatly enhanced efficacy in vitro and in vivo. Thus, this work provides a strategy to fabricate NMOFs nanocomposites with size tunability and flexible surface chemistry for various applications.

■ ASSOCIATED CONTENT

ⓢ Supporting Information

The Supporting Information is available free of charge on the ACS Publications website at DOI: 10.1021/acsami.7b10064.

> (Figures S1 and S5) Particle size distribution, (Figures S2−S4) SEM images, (Figure S6) ζ potential, (Figure S7) Fourier transform infrared spectra, (Figure S8) powder X-ray diffraction patterns, (Figures S9−S12) TEM, HRTEM, and STEM images, (Figure S13) SEM, TEM, and XRD, (Figure S14) conjugation digital image, (Figure S15) biodistributions, and (Figure S16) complete blood counts (PDF)

■ AUTHOR INFORMATION

Corresponding Authors
*(X.C.) E-mail Xianfeng.Chen@oxon.org; Michael.Chen@ed.ac.uk.
*(W.Z) E-mail: apwjzh@cityu.edu.hk.

ORCID ⓘ
Xianfeng Chen: 0000-0002-3189-2756
Vellaisamy A. L. Roy: 0000-0003-1432-9950
Wenjun Zhang: 0000-0002-4497-0688

Notes
The authors declare no competing financial interest.

■ ACKNOWLEDGMENTS

■ REFERENCES

(1) Furukawa, H.; Cordova, K. E.; O'Keeffe, M.; Yaghi, O. M. The Chemistry and Applications of Metal-Organic Frameworks. *Science* **2013**, *341*, 1230444.

(2) Yaghi, O. M.; O'Keeffe, M.; Ockwig, N. W.; Chae, H. K.; Eddaoudi, M.; Kim, J. Reticular Synthesis and The Design of New Materials. *Nature* **2003**, *423*, 705−714.

(3) Zhou, H.; Long, J. R.; Yaghi, O. M. Introduction to Metal-Organic Frameworks. *Chem. Rev.* **2012**, *112*, 673−674.

(4) Chae, H. K.; Siberio-Pérez, D.; Kim, J.; Go, Y.; Eddaoudi, M.; Matzger, A. J.; O'Keeffe, M.; Yaghi, O. A Route to High Surface Area, Porosity and Inclusion of Large Molecules in Crystals. *Nature* **2004**, *427*, 523−527.

(5) Deng, H.; Doonan, C. J.; Furukawa, H.; Ferreira, R. B.; Towne, J.; Knobler, C. B.; Wang, B.; Yaghi, O. M. Multiple Functional Groups of Varying Ratios in Metal-Organic Frameworks. *Science* **2010**, *327*, 846−850.

(6) Furukawa, H.; Ko, N.; Go, Y. B.; Aratani, N.; Choi, S. B.; Choi, E.; Yazaydin, A. O.; Snurr, R. Q.; O'Keeffe, M.; Kim, J.; Yaghi, O. M. Ultrahigh Porosity in Metal-Organic Frameworks. *Science* **2010**, *329*, 424−428.

(7) Deng, H.; Grunder, S.; Cordova, K. E.; Valente, C.; Furukawa, H.; Hmadeh, M.; Gándara, F.; Whalley, A. C.; Liu, Z.; Asahina, S.; Kazumori, H.; O'Keeffe, M.; Terasaki, O.; Stoddart, J. F.; Yaghi, O. M. Large-Pore Apertures in a Series of Metal-Organic Frameworks. *Science* **2012**, *336*, 1018−1023.

(8) DeCoste, J. B.; Peterson, G. W. Metal-Organic Frameworks for Air Purification of Toxic Chemicals. *Chem. Rev.* **2014**, *114*, 5695−5727.

(9) Li, J. R.; Kuppler, R. J.; Zhou, H. C. Selective Gas Adsorption and Separation in Metal- Organic Frameworks. *Chem. Soc. Rev.* **2009**, *38*, 1477−1504.

(10) Barea, E.; Montoro, C.; Navarro, J. A. Toxic Gas Removal–Metal-Organic Frameworks for The Capture and Degradation of Toxic Gases and Vapours. *Chem. Soc. Rev.* **2014**, *43*, 5419−5430.

(11) Suh, M. P.; Park, H. J.; Prasad, T. K.; Lim, D. W. Hydrogen Storage in Metal-Organic Frameworks. *Chem. Rev.* **2012**, *112*, 782−835.

(12) Eddaoudi, M.; Sava, D. F.; Eubank, J. F.; Adil, K.; Guillerm, V. Zeolite-Like Metal− Organic Frameworks (ZMOFs): Design, Synthesis, and Properties. *Chem. Soc. Rev.* **2015**, *44*, 228−249.

(13) Yang, Q.; Liu, D.; Zhong, C.; Li, J. R. Development of Computational Methodologies for Metal-Organic Frameworks and Their Application in Gas Separations. *Chem. Rev.* **2013**, *113*, 8261−8323.

(14) Chaemchuen, S.; Kabir, N. A.; Zhou, K.; Verpoort, F. Metal-Organic Frameworks for Upgrading Biogas via CO₂ Adsorption to Biogas Green Energy. *Chem. Soc. Rev.* **2013**, *42*, 9304−9332.

(15) Kreno, L. E.; Leong, K.; Farha, O. K.; Allendorf, M.; Van Duyne, R. P.; Hupp, J. T. Metal- Organic Framework Materials as Chemical Sensors. *Chem. Rev.* **2012**, *112*, 1105−1125.

(16) Rocha, J.; Carlos, L. D.; Paz, F. A.; Ananias, D. Luminescent Multifunctional Lanthanides- Based Metal-Organic Frameworks. *Chem. Soc. Rev.* **2011**, *40*, 926−940.

(17) Corma, A.; García, H.; Llabrés i Xamena, F. X. Engineering Metal Organic Frameworks for Heterogeneous Catalysis. *Chem. Rev.* **2010**, *110*, 4606−4655.

(18) Yoon, M.; Srirambalaji, R.; Kim, K. Homochiral Metal-Organic Frameworks for Asymmetric Heterogeneous Catalysis. *Chem. Rev.* **2012**, *112*, 1196−1231.

(19) Liu, J. W.; Chen, L. F.; Cui, H.; Zhang, J. Y.; Zhang, L.; Su, C. Y. Applications of Metal- Organic Frameworks in Heterogeneous Supramolecular Catalysis. *Chem. Soc. Rev.* **2014**, *43*, 6011−6061.

(20) Dhakshinamoorthy, A.; Garcia, H. Catalysis by Metal Nanoparticles Embedded on Metal-Organic Frameworks. *Chem. Soc. Rev.* **2012**, *41*, 5262−5284.

(21) Horcajada, P.; Gref, R.; Baati, T.; Allan, P. K.; Maurin, G.; Couvreur, P.; Férey, G.; Morris, R. E.; Serre, C. Metal-Organic Frameworks in Biomedicine. *Chem. Rev.* **2012**, *112*, 1232−1268.

(22) McKinlay, A. C.; Morris, R. E.; Horcajada, P.; Férey, G.; Gref, R.; Couvreur, P.; Serre, C. BioMOFs: Metal-Organic Frameworks for Biological and Medical Applications. *Angew. Chem., Int. Ed.* **2010**, *49*, 6260−6266.

(23) Kievit, F. M.; Zhang, M. Cancer Nanotheranostics: Improving Imaging and Therapy by Targeted Delivery across Biological Barriers. *Adv. Mater.* **2011**, *23*, H217−H247.

(24) Wang, D.; Zhou, J.; Chen, R.; Shi, R.; Xia, G.; Zhou, S.; Liu, Z.; Zhang, N.; Wang, H.; Guo, Z.; Chen, Q. Magnetically Guided Delivery of DHA and Fe Ions for Enhanced Cancer Therapy Based on pH-

Responsive Degradation of DHA-Loaded Fe3O4@C@MIL-100(Fe) Nanoparticles. *Biomaterials* **2016**, *107*, 88−101.

(25) Wang, D.; Zhou, J.; Chen, R.; Shi, R.; Zhao, G.; Xia, G.; Li, R.; Liu, Z.; Tian, J.; Wang, H.; Guo, Z.; Wang, H.; Chen, Q. Controllable Synthesis of Dual-MOFs Nanostructures for pH- Responsive Artemisinin Delivery, Magnetic Resonance and Optical Dual-Model Imaging- Guided Chemo/Photothermal Combinational Cancer Therapy. *Biomaterials* **2016**, *100*, 27−40.

(26) Zheng, H.; Zhang, Y.; Liu, L.; Wan, W.; Guo, P.; Nyström, A. M.; Zou, X. One-Pot Synthesis of Metal-Organic Frameworks with Encapsulated Target Molecules and Their Applications for Controlled Drug Delivery. *J. Am. Chem. Soc.* **2016**, *138*, 962−968.

(27) Yang, Y.; Liu, J.; Liang, C.; Feng, L.; Fu, T.; Dong, Z.; Chao, Y.; Li, Y.; Lu, G.; Chen, M.; Liu, Z. Nanoscale Metal-Organic Particles with Rapid Clearance for Magnetic Resonance Imaging-Guided Photothermal Therapy. *ACS Nano* **2016**, *10*, 2774−2781.

(28) Liu, J.; Yang, Y.; Zhu, W.; Yi, X.; Dong, Z.; Xu, X.; Chen, M.; Yang, K.; Lu, G.; Jiang, L.; Liu, Z. Nanoscale Metal-Organic Frameworks for Combined Photodynamic&Radiation Therapy in Cancer Treatment. *Biomaterials* **2016**, *97*, 1−9.

(29) Horcajada, P.; Serre, C.; Vallet-Regi, M.; Sebban, M.; Taulelle, F.; Férey, G. Metal- Organic Frameworks as Efficient Materials for Drug Delivery. *Angew. Chem., Int. Ed.* **2006**, *45*, 5974−5978.

(30) Horcajada, P.; Serre, C.; Maurin, G.; Ramsahye, N. A.; Balas, F.; Vallet-Regí, M.; Sebban, M.; Taulelle, F.; Férey, G. Flexible Porous Metal-Organic Frameworks for a Controlled Drug Delivery. *J. Am. Chem. Soc.* **2008**, *130*, 6774−6780.

(31) deKrafft, K. E.; Xie, Z.; Cao, G.; Tran, S.; Ma, L.; Zhou, O. Z.; Lin, W. Iodinated Nanoscale Coordination Polymers as Potential Contrast Agents for Computed Tomography. *Angew. Chem., Int. Ed.* **2009**, *48*, 9901−9904.

(32) Allendorf, M. D.; Bauer, C. A.; Bhakta, R. K.; Houk, R. J. Luminescent Metal-Organic Frameworks. *Chem. Soc. Rev.* **2009**, *38*, 1330−1352.

(33) Zhuang, J.; Kuo, C.; Chou, L.; Liu, D.; Weerapana, E.; Tsung, C. Optimized Metal- Organic-Framework Nanospheres for Drug Delivery: Evaluation of Small-Molecule Encapsulation. *ACS Nano* **2014**, *8*, 2812−2819.

(34) He, C.; Lu, K.; Liu, D.; Lin, W. Nanoscale Metal-Organic Frameworks for The Co- Delivery of Cisplatin and Pooled siRNAs to Enhance Therapeutic Efficacy in Drug-Resistant Ovarian Cancer Cells. *J. Am. Chem. Soc.* **2014**, *136*, 5181−5184.

(35) Zhao, D.; Tan, S.; Yuan, D.; Lu, W.; Rezenom, Y. H.; Jiang, H.; Wang, L.; Zhou, H. Surface Functionalization of Porous Coordination Nanocages via Click Chemistry and Their Application in Drug Delivery. *Adv. Mater.* **2011**, *23*, 90−93.

(36) Agostoni, V.; Chalati, T.; Horcajada, P.; Willaime, H.; Anand, R.; Semiramoth, N.; Baati, T.; Hall, S.; Maurin, G.; Chacun, H.; Bouchemal, K.; Martineau, C.; Taulelle, F.; Couvreur, P.; Rogez-Kreuz, C.; Clayette, P.; Monti, S.; Serre, C.; Gref, R. Towards an Improved Anti-HIV Activity of NRTI via Metal-Organic Frameworks Nano-particles. *Adv. Healthcare Mater.* **2013**, *2*, 1630−1637.

(37) Wu, Y.; Zhou, M.; Li, S.; Li, Z.; Li, J.; Wu, A.; Li, G.; Li, F.; Guan, X. Magnetic Metal- Organic Frameworks: γ-Fe2O3@MOFs via Confined in situ Pyrolysis Method for Drug Delivery. *Small* **2014**, *10*, 2927−2936.

(38) Horcajada, P.; Chalati, T.; Serre, C.; Gillet, B.; Sebrie, C.; Baati, T.; Eubank, J. F.; Heurtaux, D.; Clayette, P.; Kreuz, C.; Chang, J.; Hwang, Y. K.; Marsaud, V.; Bories, P.; Cynober, L.; Gil, S.; Férey, G.; Couvreur, P.; Gref, R. Porous Metal-Organic-Framework Nanoscale Carriers as a Potential Platform for Dug Delivery and Imaging. *Nat. Mater.* **2010**, *9*, 172−178.

(39) Park, J.; Jiang, Q.; Feng, D.; Mao, L.; Zhou, H. C. Size-Controlled Synthesis of Porphyrinic Metal-Organic Framework and Functionalization for Targeted Photodynamic Therapy. *J. Am. Chem. Soc.* **2016**, *138*, 3518−3525.

(40) Bellido, E.; Hidalgo, T.; Lozano, M. V.; Guillevic, M.; Simón-Vázquez, R.; Santander-Ortega, M. J.; González-Fernández, Á.; Serre, C.; Alonso, M. J.; Horcajada, P. Heparin- Engineered Mesoporous Iron Metal-Organic Framework Nanoparticles: Toward Stealth Drug Nanocarriers. *Adv. Healthcare Mater.* **2015**, *4*, 1246−1257.

(41) Ren, H.; Zhang, L.; An, J.; Wang, T.; Li, L.; Si, X.; He, L.; Wu, X.; Wang, C.; Su, Z. Polyacrylic Acid@zzeolitic Imidazolate Frame-work-8 Nanoparticles with Ultrahigh Drug Loading Capability for pH-Sensitive Drug Release. *Chem. Commun.* **2014**, *50*, 1000−1002.